HHS Public Access

Author manuscript

Nat Commun. Author manuscript; available in PMC 2012 December 13.

Published in final edited form as:

Nat Commun. 2012 ; 3: 1033. doi:10.1038/ncomms2040.

Imaging enzyme-triggered self-assembly of small molecules inside live cells

Yuan Gao, **Junfeng Shi**, **Dan Yuan**, and **Bing Xu***

Department of Chemistry, Brandeis University, 415 South Street, Waltham, MA 02453, USA

Abstract

Self-assembly of small molecules in water to form nanofibers, besides generating sophisticated biomaterials, promises a simple system inside cells for regulating cellular processes. But lack of a convenient approach for studying the self-assembly of small molecules inside cells hinders the development of such systems. Here we report a method to image enzyme-triggered self-assembly of small molecules inside live cells. After linking a fluorophore to a self-assembly motif to make a precursor, we confirmed by ^{31}P NMR and rheology that enzyme-triggered conversion of the precursor to a hydrogelator results in the formation of a hydrogel via self-assembly. The imaging contrast conferred by the nanofibers of the hydrogelators allowed the evaluation of intracellular self-assembly; the dynamics, and the localization of the nanofibers of the hydrogelators in live cells. This approach explores supramolecular chemistry inside cells and may lead to new insights, processes, or materials at the interface of chemistry and biology.

Introduction

Driven by supramolecular interactions, e.g., hydrophobic interactions and hydrogen bonding, certain small molecules self-assemble in aqueous solution to form nanofibers (or other nanostructures) and consequently result in hydrogels.[1–5] Because of their inherent advantages, such as biocompatibility, biodegradability, and morphological resemblance of extracellular matrix (ECM), supramolecular nanofibers/hydrogels promise applications in cell culture, drug delivery, and tissue engineering, and recently have attracted increased interests in the development of new biomaterials.[6–13] Besides the incorporation of epitopes or bioactive molecules in the hydrogelators,[6,14,15] it is also important to evaluate the distribution of the nanofibers of the hydrogelators in both extracellular and intracellular environment and to understand their interactions with cellular components. Although it is relatively straightforward to introduce a fluorophore into a hydrogelator[16] for imaging the location of hydrogelators in a biological setting, it is rather difficult to distinguish individual

Correspondence and requests for materials should be addressed to B.X. bxu@brandeis.edu.

Author contributions

Y.G. and B.X. conceived and designed the experiments, Y.G., J.S., and D.Y. performed the experiments, Y.G. and B.X. analyzed the data, and Y.G. and B.X. co-wrote the paper.

The authors declare no competing financial interests: details accompany the full-text HTML version of the paper at www.nature.com/naturecommunications. Supplementary information and chemical compound information accompany this paper at www.nature.com/naturecommunications.

fluorescent hydrogelators and the corresponding nanofibers because of the little difference between the two cases. In fact, due to the limited exploration on fluorescent hydrogelators and hydrogels,[17] there is no known molecule that only exhibits fluorescence after the self-assembly to form the nanofibers.

To solve the above dilemma, we chose to design, synthesize, and characterize a new precursor of fluorescent hydrogelator for evaluating the nanofibers of the hydrogelators inside cells. We expect the precursor and the individual hydrogelators to exhibit low fluorescence and the nanofibers of the hydrogelators to display bright fluorescence. We use enzymatic hydrogelation[18,19]—a process that an enzymatic reaction to convert the precursor to the hydrogelator for forming the nanofibers/hydrogels—to produce the nanofibers in cells for several reasons. First, there is a drastic difference between extracellular and intracellular environments in enzyme distributions, which offers a reliable contrast for imaging. Second, compared to the change of pH, temperature, or ionic strength, enzymatic reaction is a biocompatible strategy that works in both extra- and intracellular environments.[20–27] Third, in enzymatic hydrogelation, while the precursors diffuse freely, the formation of the nanofibers of the hydrogelators, as a convergent process, reduces the diffusion of the hydrogelators. Fourth, enzymatic hydrogelation also provides a new way to reveal the spatiotemporal files of specific enzymes, which may help understand the interaction of the nanofibers with cellular components.

By designing and generating a precursor (**2**) of fluorescent hydrogelator (**3**), we not only determined that endoplasmic reticulum (ER) is the location of the self-assembled fluorescent hydrogelators inside live cells, but also observed the growth of the nanofibers from ER towards the edge of the cells. These results, obtained from imaging enzyme-triggered self-assembly of small molecules inside live cells, illustrates a novel approach for studying the self-assembly of small molecules inside cells, a potentially important, yet unexplored subject at the interface of supramolecular chemistry and biology.[28]

Results

Principle for imaging molecular self-assembly inside cells

Figure 1 shows the principle of the fluorescent imaging of this enzyme-triggered self-assembly process inside cells. Being observed at the focal plane of the microscope, the precursor of the hydrogelator, bearing a fluorophore and an enzyme trigger (e.g., a tyrosine phosphate residue as the substrate of alkaline phosphatase), dissolves well in water and diffuses freely to result in the homogeneous distribution of the fluorophores. Being excited, the precursors in solution emit identically in each pixel within the optical thickness of the focal plane, thus affords little contrast for imaging. In the presence of the enzyme, the precursors turn into the hydrogelators, which, at above certain concentration, self-assemble to form nanofibers and to be localized. Obviously, many hydrogelators in the nanofibers lead to the high density of fluorophores in the nanofibers, which contribute much higher fluorescence to some pixels than the rest of solution does, thus affording the excellent contrast for imaging. Overall, the condensation and localization of the fluorophores render the nanofibers themselves to be distinctly visible in fluorescent microscopy.[29–31]

Design and synthesis of the precursor

Based on the principle illustrated in Figure 1, we first designed and synthesized the precursor. Figure 2 shows the design of the precursor **2**, a combination of a fluorophore, 4-nitro-2,1,3-benzoxadiazole (NBD), and a phosphorous ester on the tyrosine residue. The NBD group is a fluorophore known to give more intense fluorescence in hydrophobic environment than in water and has found applications in the imaging of self-assembly of tubulins.[32] Thus, the use of NBD warrants a high quantum yield of the fluorophore inside the nanofibers. The dephosphorylation of **2** catalyzed by an alkaline phosphatase (ALP) affords the corresponding hydrogelator **3**, which, as a more hydrophobic molecule than the precursor, is able to self-assemble in water to form nanofibers and to result in the hydrogel. While the tetrapeptidic backbone of **3** provides the basis for intermolecular hydrogen bonding, the naphthyl group and phenyl groups (on phenylalanine) favor intermolecular aromatic-aromatic interactions. These intermolecular interactions (e.g., hydrogen bonding and hydrophobic interactions) facilitate the self-assembly and the formation of the nanofibers and the hydrogel of **3**. According to the molecular design, the synthetic process of **2** is rather straightforward. After the synthesis of the peptidic motif **1** via solid phase peptide synthesis (SPPS) through an effective Fmoc-strategy,[33] we labeled **1** with the amine-reactive fluorogenic reagent (7-chloro-4-nitro-2,1,3-benzoxadiazole (NBD-Cl)) and obtain the precursor **2** in 67% yield (Fig. 2A).

Self-assembly of fluorescent hydrogelators in vitro

After obtaining **2**, we established enzyme-triggered self-assembly of fluorescent hydrogelators *in vitro*. We used ^{31}P NMR to examine the rate of dephosphorylation of **2** and applied rheometry to determine the hydrogelation point of **3**. In the ^{31}P NMR experiment, we monitored the enzymatic dephosphorylation hourly with an acquisition time of 3 min 27 sec (256 repetitions). As shown in Figure 2B, the ^{31}P peak of the phosphorous ester almost completely disappears six hours after the addition of the enzyme, suggesting the full conversion of **2** to **3**. The rheological test (Fig. 2C) shows that the hydrogelation point emerges eight hours after the addition of the enzyme, indicating that the hydrogelation occurs after the completion of the enzymatic dephosphorylation.

The visual observation and the transmission electron micrograph (TEM) of the hydrogel agree with the process of the dephosphorylation confirmed by ^{31}P NMR and rheology. At pH 7.4 and the concentration of 0.6 wt%, **2** forms a transparent solution (Fig. 3A, left), but exhibits little fluorescence (Supplementary Fig. S1A and B). Four hours after the addition of ALP (20 U/mL), the solution still shows little fluorescence. The mixture finally becomes a transparent and fluorescent hydrogel (Fig. 3A, right and Supplementary Fig. S1C and D) eight hours after the addition of the enzyme. Negative staining TEM[34] of the hydrogel of **3** reveals that the self-assembled nanofibers with quite uniform diameters (10±2 nm) entangle with each other to form a network as the matrices of the hydrogel (Fig. 3B). These results not only show that **3** self-assemble to form nanofibers, but also indicate that the formation of nanofibers (or hydrogelation) enhances the fluorescent signal of NBD.

The enhanced fluorescence of NBD in the hydrogel arises from the higher quantum yield of NBD in a hydrophobic environment.[35] According to the fluorescent spectra of the solution

of **2** (Supplementary Fig. S2), the fluorescence of **2** decreases with the increase of its concentration, suggesting that the self-quenching likely originates from the increase of the concentration of **2**. At the concentration of 0.6 wt% (5.92 mM) in an aqueous solution, the fluorophore NBD fluoresces little because of the hydrophilic environment and self-quench phenomenon. During the transition from solution to hydrogel, hydrogelators of **3** self-assemble to form nanofibers. Along either the longitudinal direction or axial direction, the dimensions of these nanofibers are larger than the two layers of **3**; thus, many molecules of **3** must embed inside the nanofibers that provide a hydrophobic microenvironment (Supplementary Fig. S3), which allows NBD to fluoresce with a higher quantum yield than in aqueous solution. In addition, the formation of the nanofibers also reduces the diffusion-originated non-irradiative decay. Therefore, the overall effect is that the hydrogel of **3** exhibits fluorescence despite that self-quenching also occurs in the nanofibers of **3** (Supplementary Fig. S4). This result validates the choice of NBD as the fluorophore of the hydrogelators.

Although the hydrogelation is, probably, the easiest way to identify molecular self-assembly in water, the self-assembly to form the nanofibers could occur without the formation of a bulk hydrogel. Thus, the fluorescence associated with the nanofibers of **3** may serve as a useful and more sensitive assay than hydrogelation for reporting the formation of the nanofibers via self-assembly. To verify whether this assumption is valid, we examined the enzyme-triggered self-assembly of the fluorescent hydrogelators below the critical gelation concentration (cgc) *in vitro.* After the addition of ALP (20 U/mL) into the solution of **2** (500 μM, in PBS buffer) in which the concentration is below the cgc (2.0 mM, Supplementary Fig. S5) required for the hydrogelation of **3**, we found a significant amount of highly fluorescent micron-size regions under confocal fluorescent microscope (Fig. 3C). As noticed, these spots hardly move and remain in the solution of **3**. These spots exhibit excellent contrast to the background, suggesting they compose of localized and concentrated **3**. While TEM of the negative-stain solution of **2** at 500 μM shows no aggregates (Supplementary Fig. S6), the TEM of the above sample of **3** reveals that these regions contain nanofibers with the length of several microns and the width of 8±2 nm as shown in Figure 3D (Supplementary Fig. S7 for the full scope of the spots). The dimensions of the nanofibers networks are similar to the sizes of the spots shown in Figure 3C. Thus, the observed fluorescence serves as the indication for the formation of the nanofibers formed by the self-assembly of **3**. In addition, the static light scattering of the solution of **2** exhibits little scattering, but the signal of scattering increases dramatically after the addition of ALP. This result (Supplementary Fig. S8) agrees with the observation from TEM and fluorescence.

Self-assembly of fluorescent hydrogelators in live cells

Since the self-assembly of **3** results in nanofibers that fluoresce much brighter than the rest of unassociated molecules of **2** or **3**, **2** is a valid candidate for studying molecular self-assembly of small molecules in cells. The *in vitro* test described above, which shows that 500 μM of **3** affords self-assembled nanofibers network, suggests that 500 μM of **3** is sufficient for intracellular formation of nanofibers. Additionally, our previous results show that the minimum concentration required for intracellular hydrogelation of a similar

compound is around 1/4 of the cgc of the hydrogelator in the buffer (without cells).[24] Moreover, the cell viability test shows that **2** has little cytotoxicity to HeLa cells even at 500 μM and over the period of three days (Supplementary Fig. S9), indicating that **2** and **3** are suitable candidates for the construction of nanomaterials inside cells for further exploration. So we incubated HeLa cells with **2** at two concentrations: 500 μM and 50 μM. Since the latter is far below the minimum concentration for hydrogelation in cells, it serves as the negative control of the formation of nanofibers and the hydrogelation. While the concentration of **2** barely changes outside the cells, **2** turns into **3** continuously inside cells, which reaches a non-equilibrium steady state. Because of the variation of the copy numbers of phosphatases in cells, it is impossible to synchronize the enzymatic conversion. Therefore, we observed the dynamics of **3** inside a single live cell in real time by recording the fluorescent images of these live cells at different time point after the addition of **2** to the cell culture (Fig. 4, Supplementary Movie 1).

Fluorescent imaging shows the accumulation of fluorophores at different rates and characteristics at those two concentrations (500 μM and 50 μM). After the addition of 500 μM of **2** to the cells, the emission of **2** outside cells remains dim during the whole experiment, which provides a clear background and enables the real-time visualization of the development of fluorescence inside live cells. The cells incubated with **2** become slightly fluorescent within 80 sec, and a bright fluorescent area appears near the nucleus in one of the cells after 3 min. After 5 min, all the cells glow brighter at the center of cytoplasm than around the outer membrane of the cells. This localized fluorescence not only indicates the formation of the nanofibers/hydrogels inside live cells (which is much faster than *in vitro* experiment), but also qualitatively suggests that the total phosphatase activity is much higher inside live cells than the concentration (20 U/mL) used in the *in vitro* experiment. On the other hand, in the cells treated with 50 μM of **2**, the fluorescence emission intensity changes little inside cells; instead the membrane is slightly brighter than the cytoplasm, which is normal and mainly due to the membrane at the orthogonal to the image plane.[30] If the fluorescence of NBD at 500 μM incubation concentration of **2** were due to the binding of **2** or **3** to hydrophobic pockets somewhere in the cell, we would observe strong fluorescence when the cell was incubated at 50 μM of **2**. The lack of strong fluorescence inside the cell at 50 μM of **2** excludes the possibility that the observed fluorescence, at 500 μM of **2,** originates from non-specific binding to hydrophobic pockets of intracellular biomembranes or only dephosphorylation.

The most notable observation in the case of 500 μM of **2** is that the increase of the brightest fluorescent area centers inside cytoplasm and the fluorescence emerges from the center of the cytoplasm toward the edge of the cells, a direction opposite to the diffusion of **2** into the cells. Since the fluorescence increases against the concentration gradient of **2** and the *in vitro* test proves that the self-assembly of **3** results in the fluorescence, the bright fluorescence suggests the self-assembly of **3** at the center of the cytoplasm. Moreover, because the formation of **3** requires the dephosphorylation of **2** catalyzed by phosphatases, the bright spots also reveal the distribution of phosphatases inside cells. Self-assembly of **3** is concentration dependent and occurs around sub mM for a significant formation of molecular aggregate. Since the concentration at this range would cause most of organic dyes to self-

quench, we have identified that the optimal concentration of **3** for cellular application is 500 μM based on fluorescence spectrum study of a serial dilution of **2** and **3**. This result suggests that care should be paid to find out optimized conditions/concentration for cellular applications.

Self-assembly originates from the endoplasmic reticulum

It is also worth to mention that although the self-assembly of **3** initiates sporadically among these cells, the spatial profiles are quite similar, that is, nearby the nucleus and in the region of endoplasmic reticulum (ER). Thus, most of the self-assembly of **3** occurs at the ER. This presumption is consistent with the cell fraction experiment (Fig. 5A), which shows that the ER containing cell fraction triggers the fastest hydrogelation (Fig. 5B) among the cell fractions.[36] In another experiment, we incubated the HeLa cells with **2** (500 μM) for 1 hour before subjecting the cell to fractionation. The TEM images of the fractions **N**, **M**, and **P** of the treated cell show substantial amount of nanofibers, suggesting the formation of the nanofibers inside cells (Fig. 6). Although the TEM of fraction **N** shows the nanofibers of **3**, the image in Figure 4 excludes the possibility that the nanofibers of **3** exist in the nucleus. Since the formation of the nanofibers of **3** is protein tyrosine phosphatase (PTP1B)-dependent and there is no report of PTP1B in the mitochondria of HeLa cells, it is unlikely that the nanofibers of **3** form inside mitochondria. Thus, the observation of the nanofibers in fractions **N** and **M** likely originates from the high molecular weight of the nanofibers of **3** that makes them more prone to sedimentation. Moreover, the observed nanofibers unlikely are microtubules because no similar nanofiber exists in the control (i.e., HeLa cells without incubating with **2**).

Since PTP1B is a phosphatase known to localize at the cytoplasmic face of the ER,[37] we used an inhibitor of PTP1B (CinnGEL 2Me, 25 μM) to co-incubate with the HeLa cells and the precursor (**2**). We observed the delay of the fluorescence (Fig. 7). For example, at 7.5 min, there is no fluorescent cell when the PTP1B inhibitor presents in the medium. After one hour incubation, 70% cells are fluorescent without the co-incubation of the PTP1B inhibitor, but only 21% cells are fluorescent in the presence of the PTP1B inhibitor. This result confirms that PTP1B is the major phosphatase that catalyzes the dephosphorylation of **2** to result in the formation of the nanofibers of **3** in the ER. The rate difference for the *in vivo* experiment and the *in vitro* (i.e., ^{31}P-NMR) experiment may arise from the concentration and activity difference of the phosphatases *in vivo* and *in vitro*. The activity of ALP purchased (Biomatic Co., A1130) has a activity of 3,000 U/mg; the PTP 1B localized at ER and has an activity of 46,780 U/mg (soluble fractions) or 42,710 U/mg (particulate fractions)[38] (1 Unit = release of 1 nmol phosphate per minute). Since the activity of PTP1B is about 15 times higher than that of ALP, it is reasonable that the dephosphorylation of **2** inside cells occurs one order of magnitude faster than *in vitro*.

Discussion

This work, as the first example that combines fluorescence, enzymatic reactions, and self-assembly, provides a minimum model structure for studying the self-assembly of small molecules inside cells, which involves cellular processes to construct the designed

nanostructures *in situ*. Though it is unable to determine the location of the nanofibers in the cells, the fractionation experiment unambiguously confirms the formation of the nanofibers inside the cells. By inhibiting the phosphatase (i.e., PTP1B) with a known cellular location (i.e., ER), we are able to infer the location of the nanofibers. Therefore, this work demonstrates the construction of nanostructures via enzyme-triggered supramolecular self-assembly inside live cells without forming the covalent bond. This approach could be applied to self-assembly triggered by other enzymes when the distribution of the enzymes is well defined.

In addition, the resulted molecular nanostructure bears the intrinsic advantages of reversibility and bio-degradability, which fundamentally differs from the result reported by Rao *et al.*,[29] in which furin initiates the reaction among precursors and results in covalently linked fluorescent oligomers inside cells. Although the increase of the local concentration of fluorescent gelators in the nanofibers of some organogels[39,40] results in improved contrast enhancement, we found that the choice of fluorophore is crucial because the replacement of NBD by rhodamine fails to provide the contrasts for imaging because the rhodamine derivative is a non-gelator. Since many critical biological processes and targets are intracellular, the understanding of the evolution of the nanofibers inside cells promises the development of intracellular biomaterials that interact with biological entities. Moreover, because the fluorescence intensity correlates with the formation of the nanofibers inside cells, this molecule may serve as a model system in a phenotype assay to screen the inhibitors of fibrillar aggregates inside cells, which ultimately may provide leads for develop drugs for neurodegenerative diseases.

Methods

Materials

Alkaline phosphatase (ALP) was purchased from Biomatik USA, LLC., and 7-chloro-4-nitro-2,1,3-benzoxadiazole (NBD-Cl) was purchased from TCI.

General

1 and **2** were purified by a Waters Delta600 HPLC system equipped with an in-line diode array UV detector using a XTerra C18 RP column with CH_3CN (0.1 % of TFA) and water (0.1 % of TFA) as the eluent. LC-MS was obtained on Waters Acquity ultra Performance LC with Waters MICROMASS detector. NMR spectra were monitored on a Varian 400M NMR. Rheological test was performed on an ARES-G2 rheometer. TEM micrographs were obtained on a FEI Morgagni 268 electron microscope with a 1k CCD camera (GATAN, Inc., Pleasanton, CA). Fluorescence spectra were measured on Shimadzu RF-5301-PC Fluorescence Spectrophotometer. Confocal images were obtained on a Leica TCS SP2 Spectral Confocal Microscope.

Synthesis of compounds

NapFFKYp (**1**) was prepared by solid phase peptide synthesis using 2-chlorotrity resin and the corresponding Fmoc-protected amino acids. ^{1}H NMR (400 MHz, DMSO-d_6): δ 8.37 (d, 1H), δ 8.27 (d, 1H), δ 8.20 (m, 2H), δ 8.12 (d, 1H), δ 7.85-7.71 (m, 3H), δ 7.59 (s, 1H), δ

7.46 (m, 2H), δ 7.30-7.00 (m, 15H), δ 4.61-4.34 (m, 3H), δ 4.14 (m, 1H), δ 3.534 (q, 2H), δ 3.15-3.01 (m, 2H), δ 2.99-2.86 (m, 2H), δ 2.84-2.63 (m, 4H), δ 1.48-1.14 (m, 4H), δ 1.08-0.79 (m, 2H); ^{13}C NMR (100 MHz, DMSO-d_6): δ 172.7, 171.1, 171.0, 170.5, 169.8, 137.8, 137.7, 133.9, 132.9, 131.7, 129.7, 129.2, 129.1, 128.0, 127.9, 127.6, 127.4, 127.3, 127.2, 126.2, 126.1, 125.9, 125.4, 119.2, 119.1, 106.9, 61.7, 53.9, 53.6, 53.0, 52.9, 42.2, 37.5, 37.2, 35.5, 31.9, 26.6, 22.0; ESI MS (*m/z*): $[M]^+$ calcd. for $C_{45}H_{50}N_5O_{10}P$, 851.33; found $[M+H]^+$, 852.49; found $[M-H]^-$, 850.54.

NapFFK(NBD)Yp (**2**): To a solution of **1** (50.0 mg, 58.7 μmol) and Na_2CO_3 (12.4 mg, 117.4 μmol) in H_2O was added NBD-Cl (58.7 μmol) dissolved in methanol. The mixture was stirred at 50 °C for 2 hours, and then cooled to R.T., neutralized with 10% HCl (aq). The solvent was removed under reduced pressure, and the crude product was purified by RP C18 HPLC (total yield: 67%). ^{1}H NMR (400 MHz, DMSO-d_6): δ 9.542 (s, 1H), δ 8.462 (d, 1H), δ 8.38-8.01 (m, 3H), δ 7.87-7.62 (m, 3H), δ 7.61-7.50 (d, 1H), δ 7.48-7.35 (m, 2H), δ 7.28-6.92 (m, 15 H), δ 6.35 (m, 2H), δ 4.69-4.12 (m, 4H), δ 3.54 (q, 2H), δ 3.07-2.63 (m, 8H), δ 1.79-1.18 (m, 6H); ^{13}C NMR (100 MHz, DMSO-d_6): δ 172.6, 171.4, 171.1, 170.6, 169.8, 137.7, 137.6, 133.8, 132.9, 131.7, 130.0, 129.2, 129.1, 128.0, 127.8, 127.6, 127.4, 127.3, 127.2, 126.2, 126.1, 125.9, 125.4, 119.7, 61.7, 53.8, 53.7, 52.2, 42.2, 37.5, 37.3, 35.9, 31.9, 27.3, 22.6, 20.8, 16.7; ESI MS (*m/z*): $[M]^+$ calcd. for $C_{51}H_{51}N_8O_{13}P$, 1014.33; found $[M+H]^+$, 1015.4975; found $[M-H]^-$, 1013.5474.

Negative staining

I) Solutions and supplies: 2.0 % (w/v) uranyl acetate (UA) (prepare by dissolving 200 mg UA in 10 ml of ddH_2O. Add water to tube containing UA, cover tube with foil and rotate in coldroom for several hours till fully dissolved. Filter through a 0.22 μm filter that has be pre-rinsed well with ddH_2O. Filtered stain stored at 4 °C in a foil-wrapped tube can be used for >1 year.); filter strips (prepared by cutting Whatman #1 filter paper into small slivers); grids (400 mesh copper grids coated with continuous thick carbon film ~35nm in thickness, purchased from Pacific Grid Tech. Co). ***II***) Negative Staining Protocol: ***1***. Glow discharge carbon coated grids just before use to increase their hydrophilicity. ***2***. Place sample solution on the grid (3 μL, sufficient to cover the grid surface). ***3***. Rinsing: ~10 sec later, place a large drop of the ddH_2O on parafilm and let the grid touch the water drop, with the sample-loaded surface facing the parafilm. Tilt the grid and gently absorb water from the edge of the grid using a filter paper sliver. (3 times) ***4***. (immediately after rinsing) Staining: place a large drop of the UA stain solution on parafilm and let the grid touch the stain solution drop, with the sample-loaded surface facing the parafilm. Tilt the grid and gently absorb the stain solution from the edge of the grid using a filter paper sliver. (3 times) ***5***. Allow the grid to dry in air and examine the grid as soon as possible.

Live cell imaging

HeLa cells (CCL-2, 2×10^5 in 2 mL) were firstly placed in Glass Chamber (Thermo Scientific Nunc Lab-Tek, 2-well) and cultured in Eagle's MEM (GIBCO) medium supplemented with 10% fetal bovine serum (FBS, GIBCO), 100 U ml^{-1} penicillin and 100 mg ml21 streptomycin (GIBCO) for 4 hours to allow the cell attachment. Then the HeLa cells were washed three times with PBS buffer to replace the medium with PBS buffer.

After the cell containing glass chamber was fixed on the confocal microscope stage, the PBS buffer was replaced with 1 mL solution of **2** (500 or 50 μM dissolved in PBS buffer) and thereafter fluorescent images were captured immediately in the xyt mode with a delay of 11.64 sec between frames.

Supplementary Material

Refer to Web version on PubMed Central for supplementary material.

Acknowledgements

The authors acknowledge the National Institute of Health (NIH R01CA142746), Human Frontiers Science Program (RGP0056/2008), MRSEC (DMR 0820492), start-up fund of Brandeis for funding to B. X. and Chinese Education Council Scholarship for funding to J. S. and D. Y. We thank Mr. R. Aguade and Prof. S. Fraden for the help on light scattering experiment.

References

1. Estroff LA, Hamilton AD. Water gelation by small organic molecules. Chem. Rev. 2004; 104:1201–1218. [PubMed: 15008620]
2. de Loos M, Feringa BL, van Esch JH. Design and application of self-assembled low molecular weight hydrogels. Eur.J. Org. Chem. 2005:3615–3631.
3. Sangeetha NM, Maitra U. Supramolecular gels: Functions and uses. Chem. Soc. Rev. 2005; 34:821–836. [PubMed: 16172672]
4. Ulijn RV, Smith AM. Designing peptide based nanomaterials. Chem. Soc. Rev. 2008; 37:664–675. [PubMed: 18362975]
5. Suzuki M, Hanabusa K. L-Lysine-based low-molecular-weight gelators. Chem. Soc. Rev. 2009; 38:967–975. [PubMed: 19421575]
6. Silva GA, et al. Selective differentiation of neural progenitor cells by high-epitope density nanofibers. Science. 2004; 303:1352–1355. [PubMed: 14739465]
7. Mart RJ, Osborne RD, Stevens MM, Ulijn RV. Peptide-based stimuli-responsive biomaterials. Soft Matter. 2006; 2:822–835.
8. Zhang SG. Fabrication of novel biomaterials through molecular self-assembly. Nat. Biotechnol. 2003; 21:1171–1178. [PubMed: 14520402]
9. Cui HG, Webber MJ, Stupp SI. Self-Assembly of Peptide Amphiphiles: From Molecules to Nanostructures to Biomaterials. Biopolymers. 2010; 94:1–18. [PubMed: 20091874]
10. Holmes TC, et al. Extensive neurite outgrowth and active synapse formation on self-assembling peptide scaffolds. Proc. Natl. Acad. Sci. U. S. A. 2000; 97:6728–6733. [PubMed: 10841570]
11. Lutolf MP, et al. Synthetic matrix metalloproteinase-sensitive hydrogels for the conduction of tissue regeneration: Engineering cell-invasion characteristics. Proc. Natl. Acad. Sci. U. S. A. 2003; 100:5413–5418. [PubMed: 12686696]
12. Yan CQ, Pochan DJ. Rheological properties of peptide-based hydrogels for biomedical and other applications. Chem. Soc. Rev. 2010; 39:3528–3540. [PubMed: 20422104]
13. Haines-Butterick L, et al. Controlling hydrogelation kinetics by peptide design for three-dimensional encapsulation and injectable delivery of cells. Proc. Natl. Acad. Sci. U. S. A. 2007; 104:7791–7796. [PubMed: 17470802]
14. Gao Y, et al. Enzyme-Instructed Molecular Self-assembly Confers Nanofibers and a Supramolecular Hydrogel of Taxol Derivative. J. Am. Chem. Soc. 2009; 131:13576–13577. [PubMed: 19731909]
15. Zhao F, Ma ML, Xu B. Molecular hydrogels of therapeutic agents. Chem. Soc. Rev. 2009; 38:883–891. [PubMed: 19421568]
16. Rozkiewicz DI, Myers BD, Stupp SI. Interfacial Self-Assembly of Cell-like Filamentous Microcapsules. Angew. Chem. Int. Ed. 2011; 50:6324–6327.

17. Yamaguchi S, Yoshimura L, Kohira T, Tamaru S, Hamachi I. Cooperation between artificial receptors and supramolecular hydrogels for sensing and discriminating phosphate derivatives. J. Am. Chem. Soc. 2005; 127:11835–11841. [PubMed: 16104762]
18. Hirst AR, et al. Biocatalytic induction of supramolecular order. Nat. Chem. 2010; 2:1089–1094. [PubMed: 21107375]
19. Yang ZM, et al. Enzymatic formation of supramolecular hydrogels. Adv. Mater. 2004; 16:1440–1444.
20. Krishna Kumar R, Yu X, Patil AJ, Li M, Mann S. Cytoskeletal-like Supramolecular Assembly and Nanoparticle-based Motors in a Model Protocell. Angew. Chem. Int. Ed. 2011; 50:9343–9347.
21. Williams RJ, et al. Enzyme-assisted self-assembly under thermodynamic control. Nature Nanotechnol. 2009; 4:19–24. [PubMed: 19119277]
22. Toledano S, Williams RJ, Jayawarna V, Ulijn RV. Enzyme-triggered self-assembly of peptide hydrogels via reversed hydrolysis. J. Am. Chem. Soc. 2006; 128:1070–1071. [PubMed: 16433511]
23. Yang ZM, Ma ML, Xu B. Using matrix metalloprotease-9 (MMP-9) to trigger supramolecular hydrogelation. Soft Matter. 2009; 5:2546–2548.
24. Yang ZM, Liang GL, Ma ML, Gao Y, Xu B. In vitro and in vivo enzymatic formation of supramolecular hydrogels based on self-assembled nanofibers of a beta-amino acid derivative. Small. 2007; 3:558–562. [PubMed: 17323399]
25. Yang ZM, Liang GL, Wang L, Xu B. Using a kinase/phosphatase switch to regulate a supramolecular hydrogel and forming the supramoleclar hydrogel in vivo. J. Am. Chem. Soc. 2006; 128:3038–3043. [PubMed: 16506785]
26. Yang Z, Liang G, Xu B. Enzymatic hydrogelation of small molecules. Acc. Chem. Res. 2008; 41:315–326. [PubMed: 18205323]
27. Yang ZM, Liang GL, Guo ZF, Guo ZH, Xu B. Intracellular Hydrogelation of Small Molecules Inhibits Bacterial Growth. Angew. Chem. Int. Ed. 2007; 46:8216–8219.
28. Lehn, J-M. Supramolecular Chemistry. 1 edn. Wiley-VCH: Weinheim; 1995.
29. Liang G, Ren H, Rao J. A biocompatible condensation reaction for controlled assembly of nanostructures in living cells. Nat Chem. 2009; 2:54–60. [PubMed: 21124381]
30. Lichtman JW, Conchello JA. Fluorescence microscopy. Nat. Methods. 2005; 2:910–919. [PubMed: 16299476]
31. Xie XS, Li GW. Central dogma at the single-molecule level in living cells. Nature. 2011; 475:308–315. [PubMed: 21776076]
32. Hiratsuka T, Kato T. A Fluorescent Analog of Colcemid, N-(7-Nitrobenz-2-Oxa-1,3-Diazol-4-Yl)-Colcemid, as a Probe for the Colcemid-Binding Sites of Tubulin and Microtubules. J Biol Chem. 1987; 262:6318–6322. [PubMed: 3571259]
33. Ottinger EA, Shekels LL, Bernlohr DA, Barany G. Synthesis of Phosphotyrosine-Containing Peptides and Their Use as Substrates for Protein-Tyrosine Phosphatases. Biochemistry. 1993; 32:4354–4361. [PubMed: 7682846]
34. Frado LL, Craig R. Electron-Microscopy of the Actin-Myosin Head Complex in the Presence of Atp. J. Mol. Biol. 1992; 223:391–397. [PubMed: 1738154]
35. Soltani CE, Hotze EM, Johnson AE, Tweten RK. Specific protein-membrane contacts are required for prepore and pore assembly by a cholesterol-dependent cytolysin. J Biol Chem. 2007; 282:15709–15716. [PubMed: 17412689]
36. Dopp E, et al. Subcellular distribution of inorganic and methylated arsenic compounds in human urothelial cells and human hepatocytes. Drug Metab. Dispos. 2008; 36:971–979. [PubMed: 18256204]
37. Frangioni JV, Beahm PH, Shifrin V, Jost CA, Neel BG. The Nontransmembrane Tyrosine Phosphatase Ptp-1b Localizes to the Endoplasmic-Reticulum Via Its 35 Amino-Acid C-Terminal Sequence. Cell. 1992; 68:545–560. [PubMed: 1739967]
38. Tonks NK, Diltz CD, Fischer EH. Purification of the Major Protein-Tyrosine-Phosphatases of Human-Placenta. J Biol Chem. 1988; 263:6722–6730. [PubMed: 2834386]

39. Giansante C, et al. White-Light-Emitting Self-Assembled NanoFibers and Their Evidence by Microspectroscopy of Individual Objects. J. Am. Chem. Soc. 2011; 133:316–325. [PubMed: 21182256]

40. Ajayaghosh A, Praveen VK. pi-organogels of self-assembled p-phenylenevinylenes: Soft materials with distinct size, shape, and functions. Acc. Chem. Res. 2007; 40:644–656. [PubMed: 17489541]

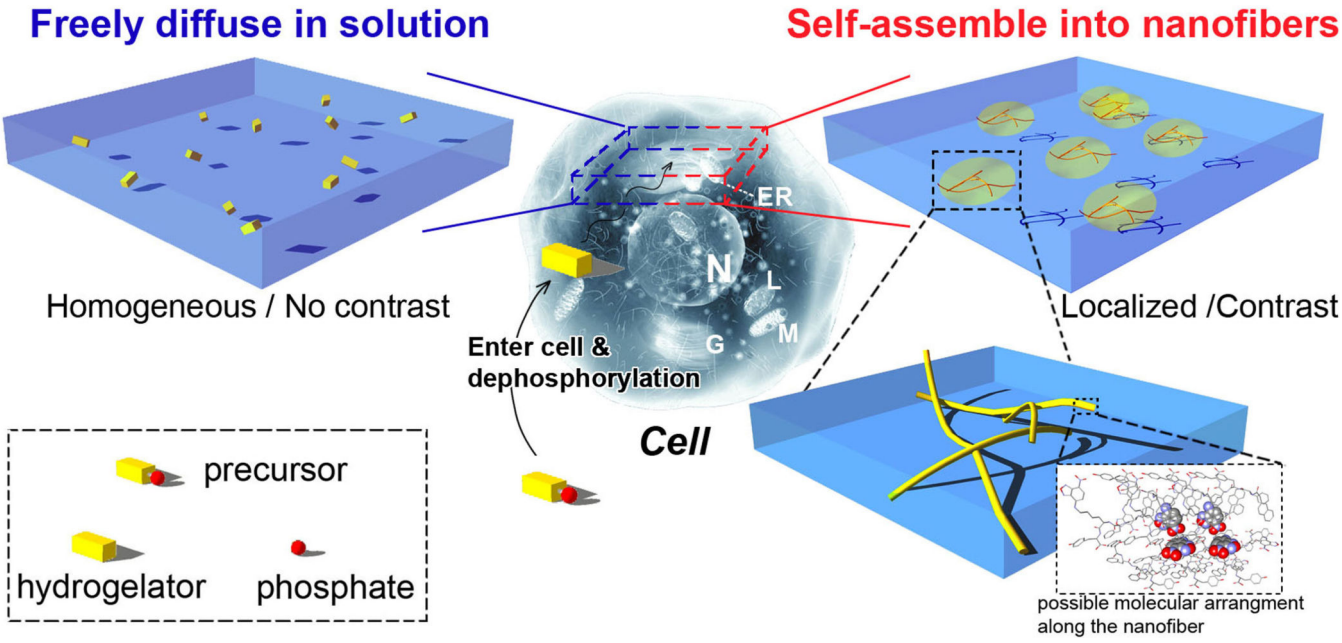

Figure 1. Principle of imaging enzyme-triggered supramolecular self-assembly inside cells

After an enzymatic conversion inside the cell, the precursor turns to the corresponding hydrogelator, a more hydrophobic molecule that self-assembles to form nanofibers at certain concentration. When the precursors are outside cells or the concentration of hydrogelator is too low to form nanofibers, those precursors or hydrogelators diffuse freely, distribute homogeneously, fluoresce identically within each pixel, and thus show little contrast. Once the concentration of hydrogelator reaches high enough to form nanofibers. These nanofibers have more fluorophores within each pixel than the rest solution, and the fluorophores (as shown in CPK model) within nanofibers are localized, therefore the nanofibers fluoresce more brightly and generate the contrast. N, nucleus; M, mitochondria; ER, endoplasmic reticulum; G, Golgi apparatus; L, lysosome.

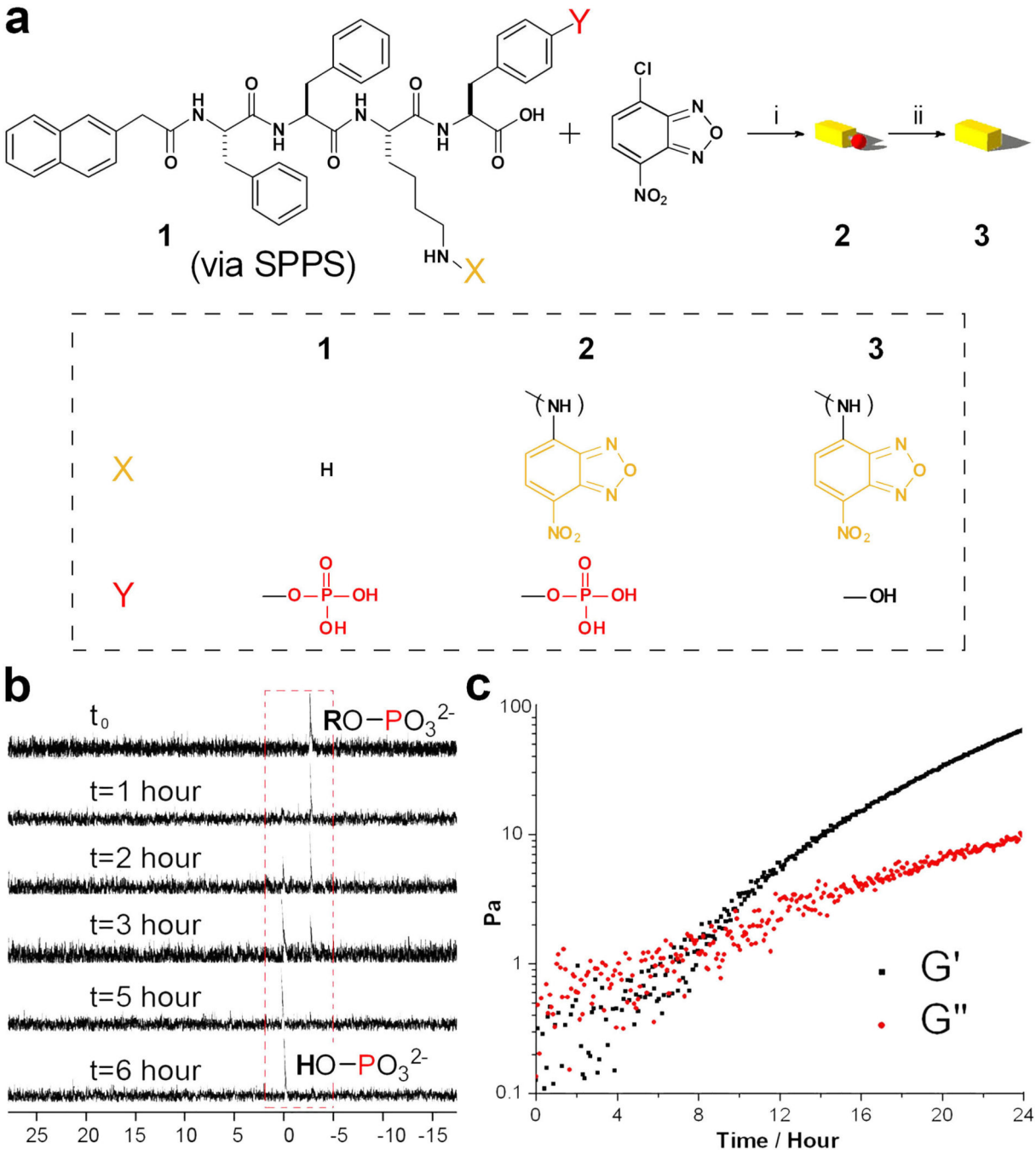

Figure 2. Molecular transformation during the enzymatic hydrogelation process

(**a**) The synthesis route of the precursor **2** and the generation of the fluorescent hydrogelator **3** via an enzyme catalyzed dephosphorylation. (**i**) Na_2CO_3, methanol, water, 50 °C, 2 hr; (**ii**) alkaline phosphatase. (**b**, **c**) The dephosphorylation and hydrogelation process of the solution of **2** (pH 7.4, 0.6 wt%, 5.92 mM) after being mixed with ALP (20 U/mL): (**b**) ^{31}P NMR to show enzymatic dephosphorylation (i.e., decrease of the phosphorous ester peak and increase of phosphate peak) and (**c**) rheometry to show the progress of the hydrogelation

of **3** that is converted from **2** (i.e., at the gel state, storage modulus (G') dominates loss modulus (G")).

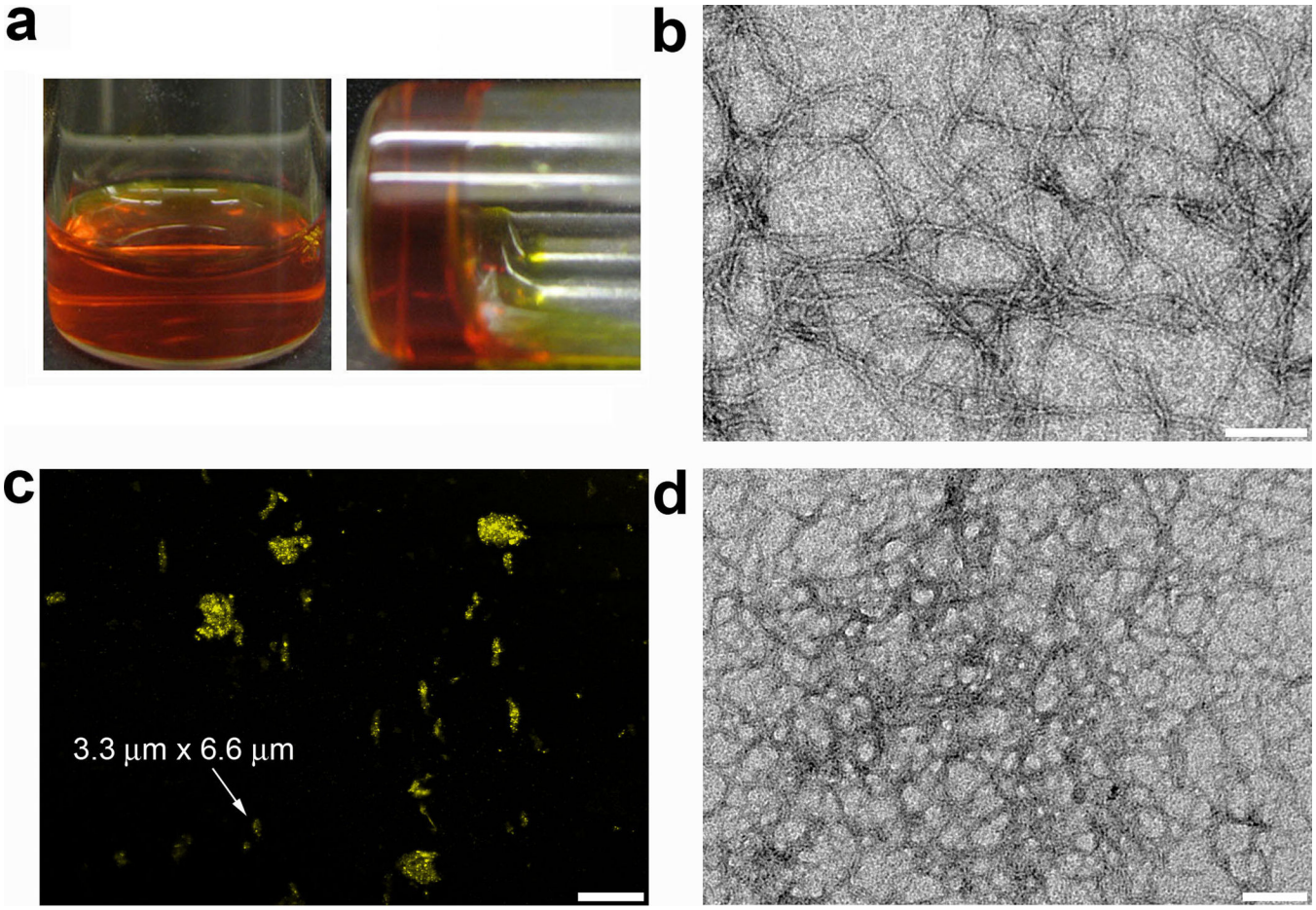

Figure 3. Enzyme-triggered self-assembly at different concentrations *in vitro*

(**a**) Optical images of (left) the solution of **2** (0.6 wt%, pH 7.4) and (right) the hydrogel of **3** by treating **2** (0.6 wt%) with ALP (20 U/mL) at pH 7.4. (**b**) The TEM image of the negatively stained nanofibers in the hydrogel of **3**. (**c**) The confocal fluorescent microscope image (63× oil objective lens) shows the appearance of bright spots in the solution of **2** (500 µM, pH 7.4 in PBS buffer) with the treatment of ALP (20 U/mL). (**d**) TEM image shows that a fluorescent spot shown in (**c**) consists of the network of nanofibers. (Scale bars: **b**, 100 nm; **c**, 25 µm; **d**, 100 nm.)

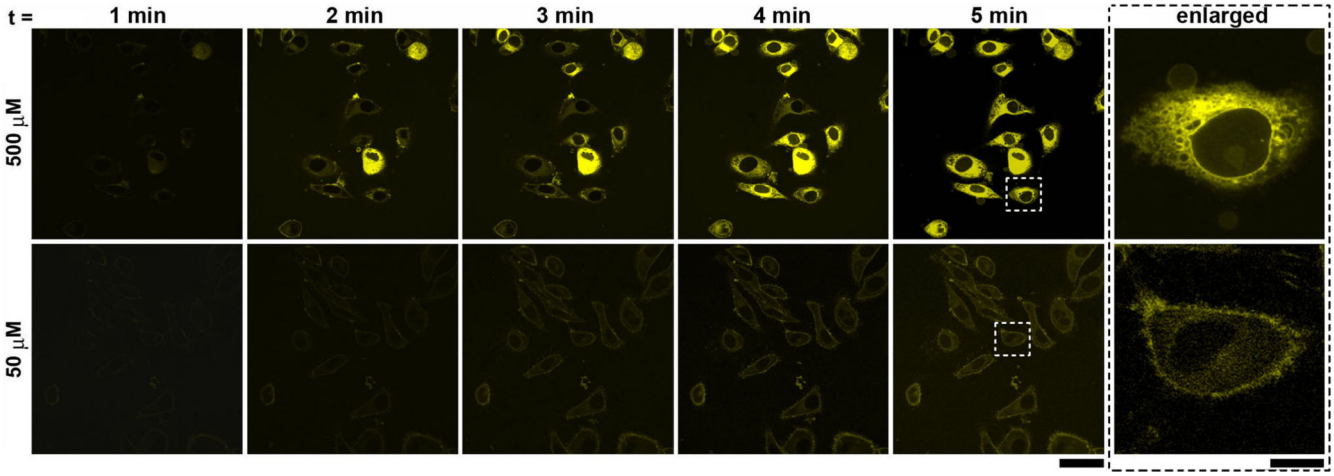

Figure 4. Enzyme-trigged self-assembly inside live cells

Fluorescent confocal microscope images show the time course of fluorescence emission inside the HeLa cells incubated with 500 μM or 50 μM of **2** in PBS buffer, which shows the different distribution of fluorophores inside living cells. Scale bars: 50 μm for time course panels and 10 μm for the enlarged panels.

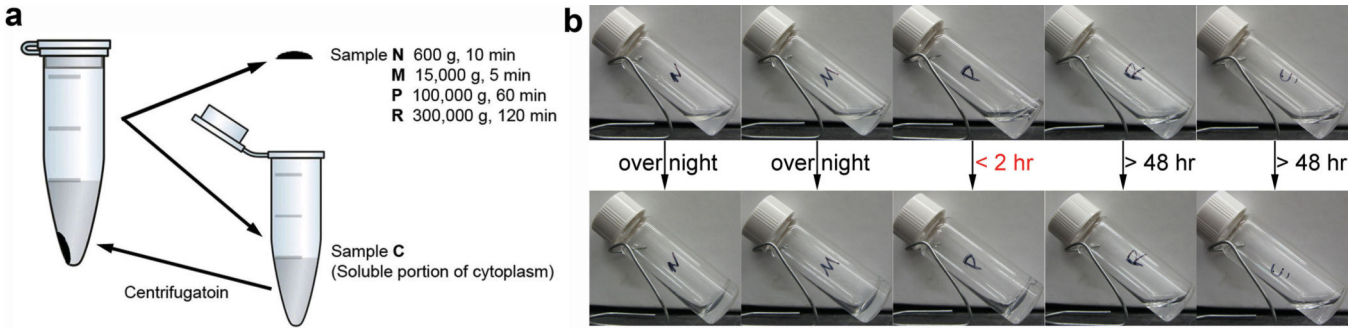

Figure 5. Cell fractionation and gelation experiments

(**a**) The cell fragmentation procedure[36] to separate pellet sample **N**: Nuclei; pellet sample **M**: Mitochondria, lysosomes, peroxisomes; pellet sample **P**: Plasma membrane, microsomal fraction (fragments of endoplasmic reticulum), large polyribsomes; pellet sample **R**: ribosomal subunits, small polyribosomes; supernatant sample **C**: soluble portion of cytoplasm (Cytosol). Pellets **N**, **M**, **P** and **R** were all re-dispersed in 200 μL of PBS for further test. (**b**) Optical images show the hydrogelation speed of each sample by mixing 100 μL of each diluted cell fraction and 200 μL of 9 mg/mL of **1** dissolved in PBS. Cell fraction **P** can induce the hydrogelation much faster (within 2 hours) than fraction **N** and **M** (overnight) while fraction **R** and **C** do not lead to a stable hydrogel.

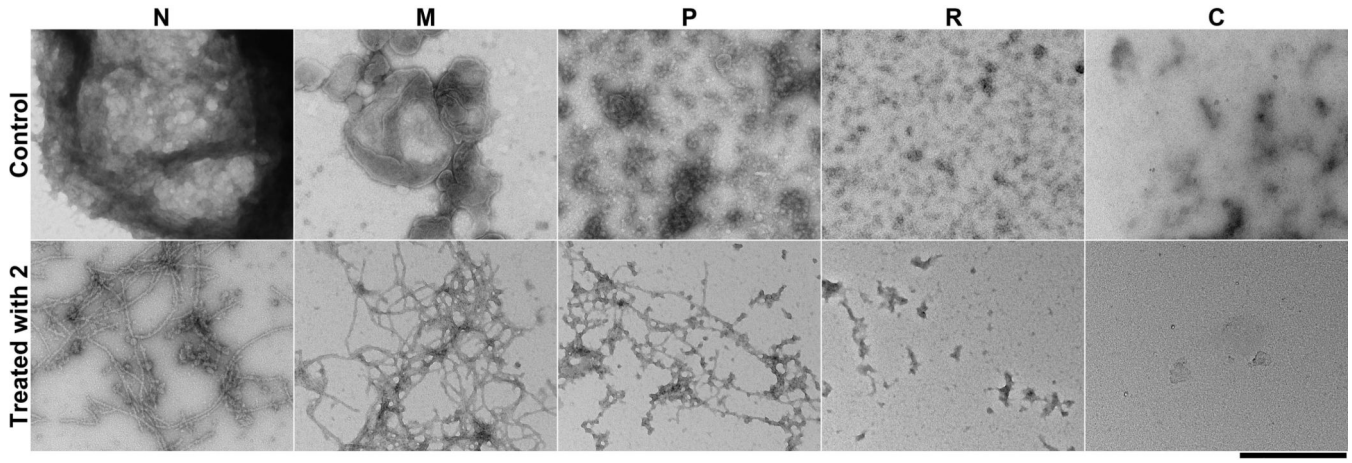

Figure 6. TEM images of the cell fractions before and after enzyme-trigged formation of the molecular nanofibers

According to the standard protocol,[36] HeLa cells were fractioned and divided into five parts, named **N**, **M**, **P**, **R**, and **C**. The first row shows the typical morphology from each fraction of HeLa cells. The second row shows the typical morphology from each fraction of HeLa cells which were pre-incubated with **2** (500 μM) for 1 hour. Scale bar: 500 nm.

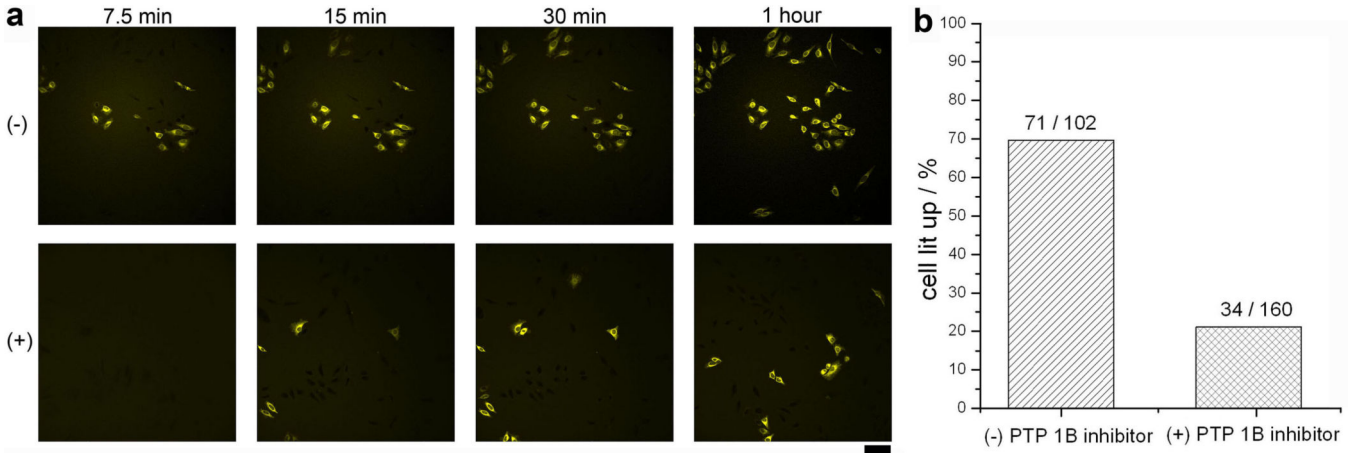

Figure 7. Protein tyrosine phosphatase 1B (PTP1B) dependent self-assembly inside live cells

(**a**) Time sequences of the HeLa cells treated with 500 μM of **2** without (−) or with (+) the PTP1B inhibitor (25 μM) (scale bar: 100 μm); (**b**) The cell count shows the difference of the percentage of fluorescent cells without and with the PTP1B inhibitor at the point of one hour after the addition of 500 μM of **2**; 71/102 means 71 cells are fluorescent in the total of 102 cells.